Spaceborne Radar Measurements of Rainfall Vertical Velocity

Eastwood Im[a], Simone Tanelli[b], Dino Giuli[b], Stephen L. Durden[a], Luca Facheris[b]

[a] Jet Propulsion Laboratory, California Institute of Technology, Pasadena CA, USA
[b] Dip.Ing.Elettronica, Universita' di Firenze, Firenze, Italy

ABSTRACT

This paper studies the performance of a spaceborne precipitation radar in measuring vertical Doppler velocity of rainfall. As far as a downward pointing precipitation radar is concerned, one of the major problems affecting Doppler measurement at the nadir direction arises from the Non-Uniform Beam-Filling effect (NUBF). That is, when significant variation in rain rate is present within the radar IFOV in the along track direction. the Doppler shift caused by the radial component of the horizontal speed of the satellite is weighted differently among the portions of IFOV. The effects of this non-uniform weighting may dominate any other contribution. Under this condition, shape, average value and width of the Doppler spectrum may not be directly correlated with the vertical velocity of the precipitating particles. However, by using an inversion technique which over-samples the radar measurements in the along track direction, we show that the shift due to NUBF can be evaluated, and that the NUBF induced errors on average fall speed can be reduced.

1. INTRODUCTION

Atmospheric scientists have recognized the importance of vertical motion at all scales of atmospheric circulations, from planetary scale down to microscale. Extensive research has gone into developing observational methods that can describe the vertical motion field and the atmospheric processes that either directly or partially correlate to vertical velocity. These include such phenomena as convective mass fluxes in the form of updrafts and downdrafts, microphysical nucleation and growth of hydrometeors, and latent heating through dynamical controls on the gravitational-driven vertical mass flux of precipitation. Many of these processes are not well understood and yet fundamental to how Earth's general circulation and climate is forced through diabatic heating controls on large scale north-south and east-west circulations, as well as mesoscale circulations.

The major atmospheric heating component in the tropics, sub-tropics and in portions of mid-latitude baroclinic waves is diabatic heating, and in conjunction with that quantity, the dominant term is latent heating. The latent heating profile is manifest in both microphysical processes (cloud-rain formation and evaporation) and in dynamical processes (i.e., vertical updrafts and downdrafts). This mix of intensive and extensive variables is exceedingly difficult to measure directly and exceedingly costly to acquire from the ground or by aircrafts. In this context, latent heat release has long stood out as one of the obscure measurements in regards to instrument makers. By the same token, with a spaceborne scanning coherent precipitation radar capable of resolving both the precipitation rate and the vertical motion field, it is possible to diagnose the latent heating field by using straightforward assumptions concerning the size and shape of hydrometeors, and the hydrodynamics of falling rain drops.

To provide such measurements, a spaceborne precipitation radar must possess the Doppler capability. Although ground-based Doppler weather radar techniques have been developed in the last two decades, they do not fully address the issues pertained to spaceborne radars. These unique issues are the downward viewing geometry with a moving orbiting platform, and the non-uniform beam-filling associated with inhomogeneous targets within a much larger observing volume. The effects of this non-uniform weighting may dominate any other contribution. Under this condition, shape, average value and width of the Doppler spectrum may not be directly correlated with the vertical velocity of the precipitating particles. In section 2 the factors affecting the characteristics of the measured signal are presented, and the resulting characteristics of the Doppler power spectrum are discussed. In section 3 the application of standard spectral moments estimators (i.e., the DFT processing and the Pulse-Pair processing) is analyzed and their performances are compared. In Section 4, a new inversion technique (CFT) which over-samples the radar measurements in the along track direction is presented. Our study shows that this new technique can significantly reduce the NUBF induced errors on the average vertical rainfall speed.

Correspondence: Eastwood Im, Jet Propulsion Laboratory, E-mail:eastwood.im@jpl.nasa.gov

2. DOPPLER SPECTRUM MEASUREMENTS FROM SPACE

Let us consider a nadir pointing spaceborne precipitation radar system orbiting at altitude h_s and a coordinate system with the x axis on the motion direction of the satellite and the z axis oriented at nadir (i.e., the radar pointing direction is given in the spherical coordinate system by $\theta=0°$). The radar observed Doppler velocity is the radial component of the relative motion of the target (i.e., rain particles) at coordinates (r, θ, ϕ) respect to the radar :

$$v_r = (v_x - v_S)\cdot\sin(\theta)\cos(\phi) + v_y\cdot\sin(\theta)\sin(\phi) + v_z\cdot\cos(\theta) \tag{1}$$

where v_x, v_y, *and* v_z (i.e., $v = [v_x, v_y, v_z]$) are the particle velocity components in the along track, cross track and vertical direction respectively,. v_S is the satellite speed. Since the typical v_S of 7 km/s is about 3 orders of magnitude higher than the typical precipitating particles velocities, the contribution of the first term of Eq. (1) may be predominant even for a small radar beamwidth θ_{3dB} (θ_{3dB} is defined as the one-way beamwidth hereinafter). As noted in Ref 4, the surfaces at constant Doppler shift (isodops) are given by the family of cones with vertices at the spacecraft and generating axes along x. Since most spaceborne precipitation radars have θ_{3dB} that is less than 1° , the isodops are well approximated inside the main lobe by the family of planes orthogonal to the vertical plane of flight of the satellite. In this case, the radial velocity can be well approximated as:

$$v_r = (v_s / h_s)x + v_z \tag{2}$$

Since the observed radial velocity Doppler spectrum consists of contributions from different relative speeds within the radar antenna beamwidth, the power spectrum, therefore, can be represented as:

$$P(v_s, r_0, f) = \int_{r_1}^{r_2}\int_0^{\pi}\int_0^{2\pi} \eta(r, f - f')W(r - r_0)r\sin\theta\, d\phi\, d\theta\, dr \tag{3}$$

where r_1 and r_2 are the range limits of the volume of resolution centered at r_0 respect to the satellite; the function $W(r)$ includes the contribution by the radar constant, the antenna gain pattern, the range weighting function, the atmospheric attenuation and the range dispersion; $\eta(r,f)$ is the natural Doppler velocity spectrum associated with the distribution of the falling particles, and f' is the Doppler shift. From Eq. (2), f' can be approximated as:

$$f'(\theta,\phi) = qx \tag{4}$$

$$q = (2/\lambda)\cdot(v_S / h_S) \tag{4'}$$

where λ is the radar wavelength. The two major contributions to $\eta(r,f)$ are:

- the different fall speed of hydrometeors. The terminal fall speed depends on the air density, and on the type and diameter of the particles. The typical average terminal fall speed is found to be in the 2-8 m/s range in the absence of up- or down-drafts[1,2], and it is commonly approximated by a Gaussian spectrum that centers at the average vertical rainfall velocity v_R and the associated spectral width σ_1 is close to 1 m/s.
- turbulence and wind shear. Since their effects are independent, their contributions can be calculated separately. The total σ_2 associated with this phenomena ranges typically between 1 and 5 m/s [3].

The resulting natural Doppler spectrum width $\sigma_R = \sqrt{\sigma_1^2 + \sigma_2^2}$, therefore, will typically vary between 2 and 5 m/s.

2.1. Uniformly and non-uniformly filled volume

The effect of relative motion of radar to the measured precipitation field has been studied quite extensively[3,4,5] both for ground-based weather radars where the relative motion is due to the antenna rotation, and for airborne/spaceborne radars where the main contribution is due to the aircraft/spacecraft motion. In most cases the rainfall is assumed to be uniform filled within the resolution volume. That is, the rainfall drop size distribution (DSD) is assumed to be constant within the resolution volume.

For a uniform rain field (i.e. $\eta(r,f) = \eta(f)$), the total spectrum measured by a nadir-looking radar with a circularly symmetric antenna pattern can be approximated by a Gaussian function with the centroid is being determined by v_R. The corresponding spectral width σ_U can be estimated as[4] :

$$\sigma_U \equiv \frac{2}{\lambda}\sqrt{\sigma_R^2 + \frac{\theta_{3dB}^2 v_s^2}{4\ln 2}} \tag{5}$$

The horizontal width of the resolution volume for the spaceborne Precipitation Radar (PR) presently flying on TRMM (Tropical Rainfall Monitoring Mission) is about 4 km (θ_{3dB} =0.71°). A new class of spaceborne precipitation radars currently being planned will have resolution of the order of 2 km. Therfore, in order to apply Eq. (5) for spaceborne radar observations, the rain field must be horizontally uniform over a range of a few kilometers.

On the other hand, when the rainfall is not uniformly spreaded over the radar resolution volume, the Non-Uniform Beam Filling (NUBF) effects take place. Most NUBF studies[5] in open literature have been focussing on the biases that the NUBF introduces to the rain intensity estimates. In addition to rain intensity, the non-uniform $\eta(r,f)$ within the radar cell will weight differently the frequency shifts given by Eq. (4). As such, the shape of the measured spectrum will be distorted with respect to Gaussian, and the accuracy on vertical rainfall velocity estimates will be degraded. In this paper, we will discuss the the accuracy on vertical rainfall velocity estimates in the presence of NUBF.

Because isodops are orthogonal to the along-track direction, only the NUBF in the along-track direction will affect the power spectrum. Therefore, Eq. (3) is re-formulated as

$$P(f) = \int_{-\infty}^{\infty} \eta_X(x, f - qx) W_X(x) dx \tag{6}$$

to emphasize the NUBF effect. In Eq. (6), the subscript X indicates the new functionals obtained by integrating $\eta(r,f)$ and $W(r)$ of Eq. (3) in the cross-track plan. Assuming that the average rainfall speed within the IFOV is v_R and that both the natural Doppler Spectrum and the antenna pattern can be approximated by Gaussian, Eq. (6) reduces to:

$$P(f) = W_X(0)\int_{-\infty}^{\infty} z_X(x)\cdot e^{-\frac{[x'-(f-f_R)/q]^2}{2\sigma_R^2/q^2}} \cdot e^{-\frac{x^2}{2\sigma_3^2}} dx \tag{7}$$

where $z_X(x)$ is the along track reflectivity profile, $f_R = -2v_R/\lambda$, and $\sigma_3 = (h_s\theta_{3dB}/2)/(2\ln(2))$. For a typical spaceborne rain radar, σ_3 is between 1 and 1.5 km, $z_X(x)$ is at the typical scale of the small rainfall patterns (~ 1 km), while σ_R/q is typically about 100m. Therefore, Eq. (7) can be approximated further as:

$$P(f) = W_X(0)\cdot z_X((f-f_R)/q)\cdot e^{-\frac{[(f-f_R)/q]^2}{2\sigma_3^2}} \tag{8}$$

It can be seen that the observed Doppler spectrum is directly related to the along-track reflectivity profile weighed by the antenna pattern.

2.2. Power spectrum estimation through spaceborne pulsed Doppler Radar

For a short-pulse weather radar, the complex voltage sample of the return of the *n-th* pulse is given by the complex linear combination of the signals related to all the scatterers included in the volume:

$$S_n = \sum_i V_i \cdot W_{i,n} \cdot e^{-2j2\pi f_0 R_{i,n}/c} \tag{9}$$

where V_i is the complex backscattering phasor (i.e., $V_i V_i^* = \sigma_{b(i)}$ where $\sigma_{b(i)}$ is the backscatter cross section of the *i-th* particle); $W_{i,n}$ is $W(r)$ calculated for the i-th particle at the time of the *n-th* pulse; $R_{i,n}$ is the range of the particle, and f_0 is the operating frequency.

Given a finite sequence of M pulses is used during rainfall Doppler measurements, the received complex voltages $\{S_n\}$ may be considered as a realization of an ergodic stationary random process. In this case, the estimate of the power spectrum $P(f)$ is given by[1]:

$$\hat{P}(f) = \frac{1}{M}\left|\sum_{n=0}^{M-1} S_n \cdot e^{-2\pi j f T_R n}\right|^2 + \frac{N}{M} \tag{10}$$

where N is the noise power. In practice, the radar integration time is chosen such that the linear velocity of the rain

particles is essentially constant during the integration time; that is $R_i(t) = R_{0i} + v_i t$ in the time range $[t_0, t_0 + T_I]$ where R_{0i} is the range of the *i-th* particle at t_0, v_i is the relative velocity of the *i-th* particle respect to the radar, and $T_I = MT_R$ is the integration time. Furthermore, if the angle of sight of each particle doesn't change appreciably (compared to the 3dB angle of the beam) in the same time interval, the term W_i can be considered constant. Therefore, by substituting (1) in (10) and inverting the summation order, the total estimated power spectrum can be seen as the weighted summation of the power spectrums of every single precipitating particle; each one being a frequency line at $-2v_i/\lambda$.

$$\hat{P}(f) = \frac{1}{M}\left|\sum_i V_i \cdot W_i \cdot e^{-2\pi j \frac{2R_{0,i}}{\lambda}} \sum_{n=0}^{M-1} e^{-2\pi j\left(\frac{2v_i}{\lambda}+f\right)T_R n}\right|^2 + \frac{N}{M} \qquad (11)$$

Since the estimate is obtained from a finite sequence of samples, the geometrical summation does not represent the ideal frequency line $\delta(f-2v_i/\lambda)$, but its approximated version $\delta_N(f+2v_i/\lambda)$. It can be easily seen, however, that by sampling the spectrum at $f=kf_R$ where $f_R = 1/T_I$ and $k=0,\ldots,M-1$, $\delta_N(kf_R+2v_i/\lambda)=0$ for all k except for $kf_R+2v_i/\lambda=0$. Besides the windowing effect, a far more important source of error is the unknown phase term depending on $R_{0,i}$ and on the phase of V_i; its effect is a multiplicative noise generally known as 'speckle'. Speckle has been extensively studied in open literature[7,8] and it explains the typical negative exponential distribution of weather derived power spectra. Since cross correlation among $\delta_N(f+2v_i/\lambda)$ is negligible, every spectral component estimate will be affected by an error with variance equal to the actual value. By performing incoherent averaging on Q statistically independent $\{S_n\}$'s, the speckle-induced error can be reduced in terms of variance of the estimate by a factor $\sqrt{Q}$, (e.g., by means of multiple frequencies or of range avaraging).

When only discrete processing (i.e., DFT) is available, reducing windowing effects, increasing spectral resolution, and providing multiple independent sequences of pulses (in order to suppress speckle), would only require the acquisition of a large M, and therefore a long integration time T_I. Although this approach led to significant improvements in weather signal processing of ground-based weather radar measurements, further discussion is required for its application to a spaceborne pulsed preciptation radar.

Let us now assume that every component of the particle velocity v_i is constant over the pulse integration time interval T_I, then the variation of v_r (Δv_r) can be calculated through (2) by using $x = v_S T_I$. This linear time dependence of the radial velocity variation broadens the estimated power spectrum. Furthermore, in order to consider the term $W_{i,n}$ constant over T_I, the following condition must be satified:

$$\Delta\theta \equiv v_S T_I / h_s << \theta_{3dB} \qquad (12)$$

As a reasonable limit it can be assumed that the shift within T_I is less than half of the antenna IFOV[5]. As a result, the velocity resolution of the Doppler spectra cannot be reduced indefinitely by increasing T_I since this would increase also the effects of Δv_r. A tradeoff can be found by requiring a Doppler velocity resolution equal to Δv_r; under such assumption Eq. (11) is an accurate estimate of Eq. (3). It can be noted, however, that if the rainfall field is homogeneous over the observed area, such a limitation becomes unnecessary and longer integration times can be used. Furthermore, even if such a constraint is not strictly satisfied but T_I is such that (6) still holds, the basic effect is simply a further broadening of the spectrum without introducing biases.

In Table 1 the expected normalized spectral widths for some system parameter combinations are shown. The range of PRF is a trade off between the requirements in maximum unambiguous range and maximum unambiguous Doppler velocity. Within this range of parameters $\sigma_{f'}$ is determined mainly by θ_{3dB} and v_S but it has been found that, accordingly with [6], accurate (i.e., within approximately 1 m/s) estimates of the average vertical falling speed of hydrometeors v_R can still be obtained provided the normalized spectral width $\sigma_{f'} / 2f_m$ (where f_m is the max. unambiguous Doppler frequency) does not exceed $1/2\pi$ and SNR > 5.

It is evident from Eq. (8) that the NUBF-induced variations in $z_N(x)$ will introduce a bias to the first moment of $P(f)$ is affected by a bias depending on the characteristics of $z_N(x)$, and preminently on its first moment π_Z and decorrelation distance ρ_Z (defined as the minimum distance reducing the autocorrelation function at $1/e$ of its maximum value).

Furthermore, when rainfall variations within the footprint are relevant (e.g. when strong and small convective cells are present), variations in $\eta(r,f)$ of some 10-20 dBZ can be easily observed. This means that the contributions to the total spectrum related to the strong signatures in the reflectivity will be significant even if they are placed outside of the 3dB IFOV. Thus (4) leads to f' that could also exceed the maximum unambiguous Doppler frequency range adopted taking into account only the 3dB portion of the antenna beam and a standard width for the natural spectrum width.

v_S	7 km/s	θ_{3dB}	0.3°
h_S	432km	f_0	13.6 GHz
PRF	6000	M	64-128-256
v_m	33 m/s	θ_D	0.27°

Table (1): System Parameters. $v_m = (\lambda/2) * (PRF / 4)$ is the maximum unambiguous velocity, where $\lambda = c/f_0$ is the operating wavelength. The maximum unambiguous shift elevatione angle is $\theta_D = v_m/v_S$.

PRF \ θ_{3dB}	0.25°	0.3°	0.5°	0.71°
6000	0.125	0.15	0.25	0.355
7000	0.11	0.13	0.21	0.30
8000	0.095	0.11	0.19	0.27

Table (2): Normalized spectral widths as function of (*PRF* and θ_{3dB}). Values in gray allow accurate average falling speed estimates.

3. SPECTRAL MOMENTS ESTIMATORS

The two most widely used methods for spectral moments estimation of weather signals are the autocovariance processing by means of the pulse pair processor (PP) and the spectral analysis by means of DFT, or FFT when appliable, [6]. Although several other methods have been developed for estimation of the first three moments of power spectrum (see [10] for a recent proposal including overview previous methods), only the DFT approach grants the capability of identifying features different from the statistical moments and eventually editing the power spectrum for specific corrections.

When uniform filling occurs, the spectral width can be estimated a priori accordingly with (5) and, given a certain choice of PRF and M, the mean Doppler velocity can be estimated with the accuracy given by the specific method. The reader is referred to [6] and [10] for details, here only the analysis of performances for a specific configuration will be provided.

It was shown that when NUBF occurs, the resulting spectrum loses the Gaussian shape, the symmetry property and, above all, the inhomogeneous weighing of the Doppler shift due to the satellite motion creates an additional bias on mean frequency estimate. In order to provide a quantitative estimate of the accuracy achievable by classical means, Monte Carlo simulations were performed for a simplified case with the operating parameters shown in Table (2). A constant average falling speed v_0 is assumed within the whole volume of resolution, on the contrary the along track reflectivity profiles $Z_X(x)$ were generated as linear combination of a constant value plus one gaussian shaped feature with width ranging from 250m to $2\sigma_S$.

The estimated power spectrum $P(f)$ is then calculated through (8). The sampling in the time domain is simulated by taking into account the spectral folding beyond the Nyquist frequency determined by the PRF and the broadening due to satellite motion as discussed at the end of previous section. M samples P_j in the frequency domain are held and white Gaussian thermal noise $N_j = NT_S$ and multiplicative noise are then added as in [11] H times. Noisy realizations $\{\tilde{P}_j\}_M$ of the estimated spectum are therefore obtained. Again accordingly to the procedure in [11] the corresponding sequences of complex voltages in the time domain $\{s_i\}_M$ are calculated from each $\{\tilde{P}_i\}_i$. The average Doppler speed is then estimated through DFT and PP processing separately.

$$\hat{v}^{DFT} = -\frac{\lambda}{2MT_S}\left\{\hat{m}' + \frac{1}{\tilde{P}-\hat{N}}\sum_{m=\hat{m}'-M/2}^{\hat{m}'+M/2}(m-\hat{m}')\cdot\left[\tilde{P}_{\mathrm{mod}_M(j)} - \hat{N}_j\right]\right\} \tag{13}$$

where $\hat{m}'$ is an approximation to the mean spectral line (here obtained by applying the previous expression a first time with $\hat{m}' = 0$), $\tilde{P}$ is the total power of the noisy signal and $\hat{N}$ is the estimated noise power: $\hat{N} = \sum_{j=0}^{M-1}\hat{N}_j$.

$$\hat{v}^{PP} = -\frac{\lambda}{2}\frac{1}{2\pi T_S}\arg\left(\frac{1}{M-1}\sum_{k=-(M-1)/2}^{(M-1)/2-1} s_k^* s_{k+1}\right) \tag{14}$$

It is then possible to calculate for each reflectivity profile $Z_X(x)$ the estimates of bias and variance (hereafter 'var') of the average Doppler velocity estimate from the H independent estimates obtained through the previous two expressions.

In order to determine a suitable value for H and to validate the results of Monte Carlo simulations, the results were compared with the expected values obtained through application of perturbation analysis shown in [12]. Results with H =

1000 were in excellent agreement with the results of perturbation analysis shown (i.e., $bias_{MC}$ = $bias_{PA}$ ± 0.2 m/s and var_{MC} = var_{PA} ± 0.1 m/s). It was verified that the two functionals bias and var are fairly independent. Also it was confirmed that larger *M* reduce the expected var but do not affect the distribution of the bias. In effect var depends almost only on the spectrum width which in turn depends (once the parameters in Table (2) are fixed) on SNR and ρ_Z as illustrated in Fig. (1). The dependency on ρ_Z is evident only for relatively high SNR and for $\rho_Z < 2\sigma_3$, beyond that the antenna pattern is the dominating factor in determining the spectral width, for this reason, in the following reflectivity profiles with $\rho_Z > 2\sigma_3$ Will be referred to as 'quasi-uniform' beam filling cases (QUBF). In order to single out the different performances under uniform or non-uniform beam filling the QUBF samples were analyzed separately, clustering in the range form 0.8 to 1.5 is evident for M = 128 in Fig. (1). The reduction in var for low ρ_Z is due to the narrowing of the spectrum due to the presence of a feature in the reflectivity pattern smaller than the IFOV.

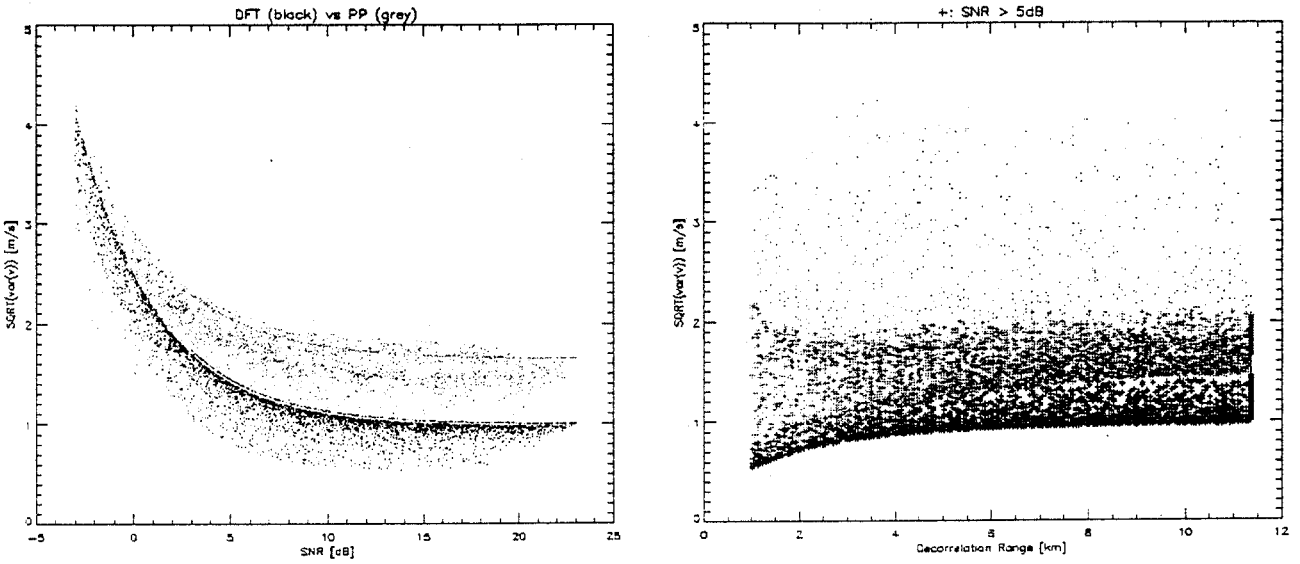

Fig. (1) Standard deviation of mean Doppler velocity estimates plotted vs SNR (left) and decorrelation range of the along track reflectivity profile (right) for 5000 different $Z_x(x)$. Pulse Pair processor performances are in grey and DFT performances are in black. Samples with SNR > 5dB are presented with a + sign in the right hand plot. Samples with uniform beam filling (i.e.. constant $Z_x(x)$) are shown as a continuous line in the left hand plot and as a thick bar at the rightmost end in the right hand plot.

Comparison of performances of FFT and PP processing is also shown. Slightly better performances in terms of var(v) are obtained through FFT processing. A different result is generally obtained when comparing the performances of these two spectral moments estimators for ground based Doppler weather radar applications: the reason of this apparent disagreement is the relatively large normalized spectral width - shown in Table (1) - and number of samples, for the spaceborne application. These two factors are recognized as improving the performances of FFT processing compared to PP [6]. Furthermore, occasional but significant increase in $var_{PP}(v)$ is observed whenever the expected power spectrum calculated through (8) loses symmetry, this is particularly evident at low ρ_Z in plot b, where the scale of the inhomogeneity is the same as the scale of the antenna pattern. Finally it has been observed that biasing effects both techniques almost equally.

The estimated overall accuracy can be then expressed as $acc(\hat{v}) = \sqrt{(bias(\hat{v}))^2 + var(\hat{v})}$ and it is plotted against $|\bar{x}_Z|$ in the left hand plot in Fig. (2). It is evident that when $|\bar{x}_Z|$ > 500m the dominating accuracy limiting factor is the bias.

The results confirm that in presence of an almost uniform rainfall field (e.g. maximum variation in Z within the IFOV lower than 3 dB below the peak value) the adopted operating parameters allow to estimate vertical motion of droplets with an accuracy of 1 m/s. As previously mentioned, the variance of the estimate can be furtherly reduced by applying more efficient sampling strategies (e.g., by means of frequency diversity as in TRMM/PR or polarization diversity) that would provide further independent sampling, useful to reduce the variance of the gaussian weather signal. Alternatively (or jointly with) mean Doppler velocity estimate variance can be reduced through more sophisticated spectral moments estimators such as those based on Maximum Likelihood principle [10].

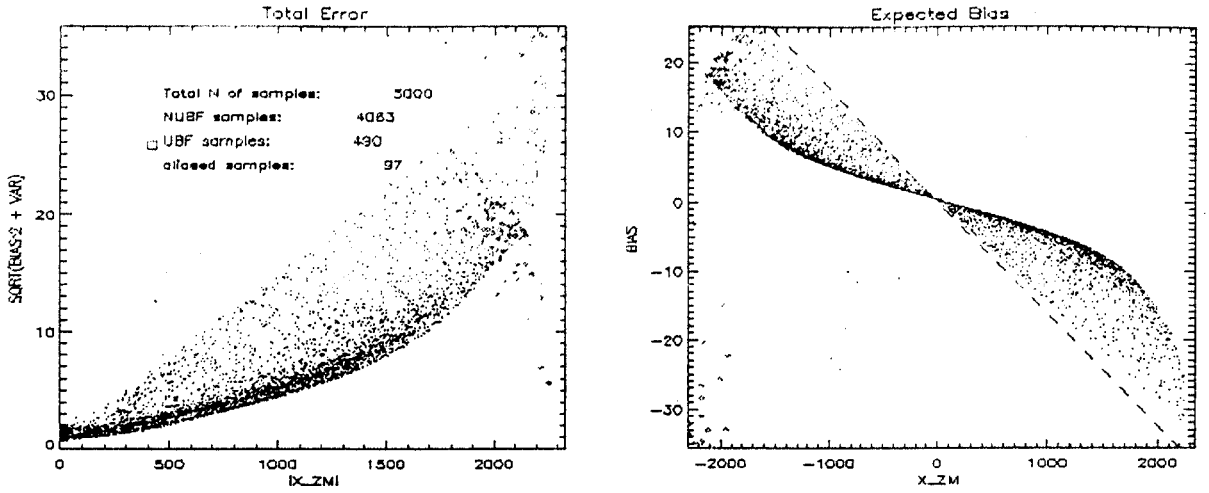

Fig. (2) Accuracy of the mean Doppler velocity estimates for 5000 different $Z_x(x)$ vs the position of the 'center of mass' of the along track reflectivity pattern, i.e., $\bar{x}_z = E[Z_X(x)]$. Left: overall accuracy accounting for variance due to speckle noise on the weather signal and for biasing due to non zero $\bar{x}_z$; right: biasing due to $\bar{x}_z$. The dashed line is the biasing that a point target at x = $\bar{x}_z$ would show in terms of Doppler velocity estimation.

On the other side, presence of NUBF makes any estimate unreliable due to the bias introduced in the spectral shape, and this term is not determined by the noisy nature of the weather signal, but rather by the unknown shape of the along-track profile of reflectivity.

In order to overcome this problem further analysis of the power spectrum is required, and to this purpose DFT processing appears to be the most suitable tool. When DFT processing is applied for this purpose a further constraint on M occurs: in order to achieve a spectral resolution significantly smaller than σ_U it would be enough to require $PRF/M << \sigma_U$, but, in presence of NUBF, the resulting narrower spectral features need to be properly sampled as well, therefore the condition is $PRF/M << min\ \{\sigma_U , q\ \rho_Z\}$.

3.1. Simulations on 3D dataset

A second simulator has been implemented mainly with the purpose of providing a better insight of the performances actually achievable by a spaceborne Doppler radar: synthetic spectra were obtained through the following procedure: the radar volume of resolution e_r is first subdivided in small volumes e_n each one having size much smaller than the resolution volume but still much larger than the operating wavelength. The volume of resolution considered is bounded by the null-null beamwidth θ_0 of the antenna beam. Antenna pattern is chosen circularly symmetric and Gaussian for $\theta < \theta_0/2$, therefore the two way gain at $\theta = \theta_0/2$ is –38dB respect to $\theta = 0$. Spectral contributions by sidelobes cannot generally be ignored for nadir looking systems, anyway they are shifted in frequency by $f_m\ cos(\phi)\ \theta / \theta_D$ (see Table (2) for symbols). For all the considered configurations $\theta_D < \theta_0/2$ therefore contribution by sidelobes can be included in the white thermal noise contribution. Antenna gain and range weighting functions are then considered constant within each e_n.

The natural spectrum of each e_n is determined taking into account the spread due to different terminal velocities, the broadening due to turbulence and wind shear, as well as the broadening due to finite integration time and satellite motion as discussed in section 2. The Doppler velocity spectrum is determined also by the shift due to the radial component of the satellite velocity calculated at the center of the small volume, and by the shift caused by average wind speed. A constant shape was assumed for DSDs (negative exponential), while the value of parameters depends only the rainfall inensity R_n of the truth reference data set at the position of the small volume. Broadening by turbulence and wind shear is constant.

Contributions from every e_n are then summed incoherently. The resulting spectrum is finally modified in order to simulate effects by 'speckle' –as discussed in Section 2 - and white noise at the receiver. Simulations were performed for a satelllite whose parameters are described in Table (2) and M = 240.

Reflectivity and average Doppler velocity measurements gathered by means of the airborne NASA/JPL Doppler weather radar were used as truth reference for this study. Resampling on a 3D cartesian grid was performed as in 5.. The event was monitored on 1993, Feb. 10th . Conversion from reflectivity to rainfall rate was performed using $Z = aR^b$ with a=372.4 and

b=1.54[5]. Finally the negative exponential DSD was calculated with $N_0=8000$ and $\Lambda=4.1R^{-0.21}$.

The ground resolution in the along-track direction resulting from the adopted parameters is 280m, therefore significant overlapping of the volumes of resolution takes place among consecutive samplings. Due to this overlapping the bias contribution to accuracy is highly correlated in the along-track direction, on the contrary the contribution by the variance term is totally uncorrelated among consecutive samples.

Along track profile of 'true' average Doppler vertical velocity is shown in Fig. (3) together with the estimates obtained by means of DFT and PP processing. The estimated profiles were also smoothed (by means of a moving window average over three samples) in order to highlight the contribution of the bias term. It can be noticed that although DFT performs slightly better in terms of overall statistics, no significant difference in terms of accuracy on the estimate can be seen. Finally, two strong correlations are evident: the one betwwen the errors of PP and DFT (confirming that NUBF affects equally both methods), and the negative one between the error and the first derivative of the along track reflectivity profile $Z_X(x)$.

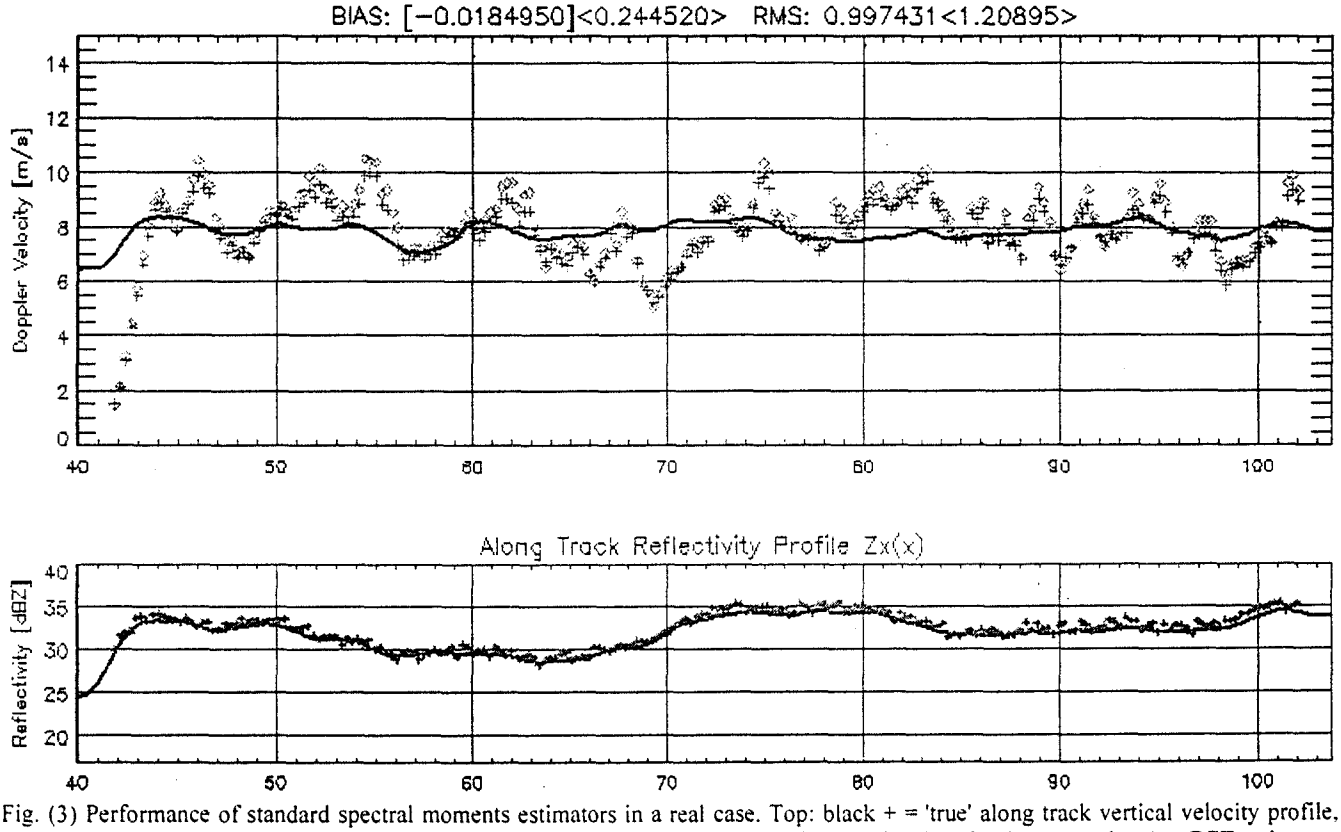

Fig. (3) Performance of standard spectral moments estimators in a real case. Top: black + = 'true' along track vertical velocity profile, grey diamonds and angle bracketed values are related to PP estimates, grey + and square bracketed values are related to DFT estimates; Bottom: black = 'true' along track reflectivity profile, grey = reconstructed along track reflectivity profile.

4. VERTICAL VELOCITY RETRIEVAL THROUGH ALONG TRACK OVERSAMPLING

In previous section it was shown that presence of NUBF in Doppler measurements from space prevents from gathering reliable estimates of precipitating particles by means of any classical spectral analysis techniques. On the other hand DFT approach may be profitably used to identify the presence of such a phenomenon.

It has been previously demonstrated that any non-homogeneity in the cross-track projection of the reflectivity pattern at a given range bin would change the shape of the observed spctrum from the Gaussian shape of predictable width that is expected under uniform filling. Anyway, when such a feature is detected, the information that can be retrieved by a single spectrum is affected by the bias effect that cannot be removed unless the $Z_X(x)$ pattern is known. This is possible by oversampling in the along-track direction, i.e., $v_S MT_R < \sigma_y/2$.

In the results discussed in the previous section $v_S MT_R = 280m$ and $\sigma_y/2 = 565m$. Correlation between $dZ_X(x)/dx$ and -err(v) is fairly evident. Although |err(v)| can locally reach values as high as 3 m/s, such localized inaccuracies can easily be

foreseen by analysis of the observed $Z_N(x)$ and removed or eventually refined through off-line postprocessing. A simple possibility is given by averaging the estimated Doppler velocity over a segment $[x_0,x_1]$ such that $Z_N(x_0) \approx Z_N(x_1)$. In this way the opposite biasing of raising Z and dropping Z slopes is used to mitigate the NUBF effect on the overall effect. The main drawback of such an approach would be the reduced and not constant along-track resolution.

In this section another method to estimate mean falling speed of hydrometeors from Doppler space measurements also when NUBF takes place is presented. It relies on the availability of measurements on partially overlapped IFOVs and on the identification and localization of high reflectivity cells within the rainfall field.

The approach relies on principles that are strongly related to the unfocussed SAR theory about the interpretation of the phase history of echoes reflected by targets moving across the beam of the radar as the satellite moves in the along track direction. The main difference being due to the fact that the 'targets' here considered are volumes filled by raindrops whose shape and velocity respect to the earth surface are not known.

If we consider the rainfall field within the volume of resolution of a nadir pointing Doppler radar as a combination of a uniform field and of some small rain cells with higher reflectivity and a rainfall intensity pattern $R_n(r)$ small compared to the IFOV. The contributions of the non uniform R_n cells will be biased in frequency by their distribution along x, therefore, in order to retrieve unbiased estimates of the average falling speed, it is necessary to estimate at the same time the positions of the $R_n(r)$.

In brief, the following aspects make the discussed application differ from SAR processing applied to earth surface monitoring from space:

- since nadir (or close to nadir) angles are chosen in order to reduce as much as possible surface clutter contributions to the weather signal, the cross track resolution is not related to range resolution but only to the cross track antenna beamwidth and eventual cross track scanning capabilities of the spaceborne weather radar;
- the velocity of targets respect to the earth surface is not known, in effect its vertical component is the unknown parameter to be estimated by means of this monitoring system, therefore Doppler parameters estimation cannot be performed in the usual way;
- longer pulses are needed since weather signals carry stronger sensitivity requirements.

4.1. Time-frequency representation and spectral front projection

It is possible to define the 1 dimensional front projection of a 2-dimensional functional, along the direction i_ρ as:

$$Q^{\perp}_{(x_0,i_\rho)}(t) = \int_{-\infty}^{\infty} Q(x_0 + ti_t + \rho i_\rho)d\rho \tag{15}$$

where $i_t \perp i_\rho$ is and x_0 is the center of projection.

Let us now consider a nadir looking spaceborne Doppler radar system whose position $x_s = 0$ at $t=0$ and with constant velocity v_S. Substituting in (6) and considering separately each range bin, we have a time-frequency representation of the Doppler velocity:

$$P_{(x_{S_0},v_S)}(t,f) = \int_{-\infty}^{\infty} \eta_N\left(x, f - q(x - v_S t)\right) W_N(x - v_S t)dx \tag{16}$$

The the slope of the 'track' in the t-f plane left by a target whose position and velocity are constant over the time the antenna beam intersects it is given by the parameter q in (4) multiplied by v_S.

Then, applying (15) to (16) with $i_\rho = [1,-q]/sqrt(1+q^2)$ and $i_t = [q,1]/sqrt(1+q^2)$, we get through simple substitutions the front projection of the time-frequency representation of the observed power spectrum:

$$P^{\perp}_{(v_{S_0},v_S)}(t) = C_W \int_{-\infty}^{\infty} \eta_N\left(v_S t + x, -qx\right)dx \tag{17}$$

where C_W is the integral value of $W_N(x)$.

By means of (17), it is possible to separate the total power contribution of all groups of targets lying on the same track in the *t-f* plane, that is, targets that show the same radial velocity respect to the radar, no matter their relative positioning.

4.2. Inversion technique for mean vertical velocity retrieval from space

Now, a radar system performing a range-Doppler frequency acquisition every T_I seconds provides a spectra stack $\underline{\underline{S}}(n,k,h)$ where the element $S_{n,k,h}$ is the Doppler spectrum line at $f=(n-N/2)/T_I$, gathered at time $T_k=kT_I$ and at the range bin h. The spectra stack, processed separately for each range layer, is the input of the inversion technique presented.

Since the inversion technique relies on the calculation of a sampled version of (17) over a constant range slice of the stack of spectra, it must be noted that (17) is calculated over a number of samples given by:

$$M_x = \frac{\lambda}{2}\frac{h_S}{(v_S T_R)^2}\frac{1}{M} \tag{18}$$

that, under the condition of $\Delta V_r = \lambda/2 * PRF/M$ discussed in section 2, becomes simply $M_x = M$.

To estimate the contribution of the uniform component of the rainfall field spectras are processed in groups as follows:

$$\underline{\underline{S_U}}(n,k,h) = G_{(u_k,\sigma_U)}(n) \quad u_k : G_{(u_k,\sigma_U)}(n) \le \underline{\underline{S}}(n,k',h) \quad \forall n \quad \forall k' \in [k-M/2, k+M/2] \tag{19}$$

where,

$$G_{(s_k,u_k,\sigma_U)}(n) = s_k \cdot e^{-\frac{[(n-N/2)\Delta f - u_k]^2}{2\sigma_U^2}} \tag{20}$$

The contribution by the locally uniform rainfield component is removed from the observed spectrum since it does not shift in frequency by small changes of *t*:

$$\underline{\underline{S_V}}(n,k,h) = \underline{\underline{S}}(n,k,h) - \underline{\underline{S_U}}(n,k,h) \tag{21}$$

Projection of S_V is then calculated accordingly with (17). Peak-like features (clusters) in the power projection $P^{\perp}(t)$ are identified and each one is associated with an element $R_n(x)$. Clustering of tracks is performed by analyzing $P^{\perp}(t)$ and its first derivative.

The target center *(t, f)* associated with each primary track - i.e., the track leding to peak values of $P^{\perp}(t)$ within a certain cluster - is determined by finding the maximum of the best fit gaussian spectrum along the. The rationale for this approach lies in the fact that if a $\delta(t,f)$ is considered as being the origin of a track its maximum intensity will be gathered when the target is closest to the maximum antenna gain direction. The gaussian fit is adopted consistently with the assumptions on the antenna pattern and in order to reduce the effects of noise (in particular speckle noise). The target centers are then associated with the corresponding $Z_X(x)$ and $v(x)$ features in the *x-v* plane:

$$x_n = v_S t_n \qquad v_n = -\frac{2}{\lambda} f_n \tag{22}$$

Secondary tracks within the clusters are also identified in order to increase spatial resolution. Secondary tracks lie between two major clusters whose centers are separated along track by more than the desired resolution. The approach to identify the target center of these clusters is identical to the one used for major clusters. Anyway, since the related total backscattered power is significantly lower, a check performed on the width of the best fitting gaussian reveals wether such estimate can be considered reliable or not: in effect the width of the best fit gaussian is strictly related to the satellite speed, larger widths indicate presence of too high contribution by noise. Target centers considered unreliable are discarded.

Target centers are finally combined in order to obtain v profile with constant spatial resolution. Linear combination of target centers is weighted by their respective total power estimates z_i, and by the functional $E_G(i)$ proportional to the relative root mean square of the gaussian fit of the track versus the true track.

$$v(x) = \sum_i v_i \cdot z_i \cdot E_G(i) \cdot W_X(x - x_i) \tag{23}$$

This technique is referred to as Combined Frequency-Time technique (CFT). A representative example of the results

obtained is shown in the following figures, comparison with standard techniques shows that the sensitivity of accuracy to the NUBF is considerably reduced and that the overall accuracy of 1 m/s can be achieved also under heavy NUBF.

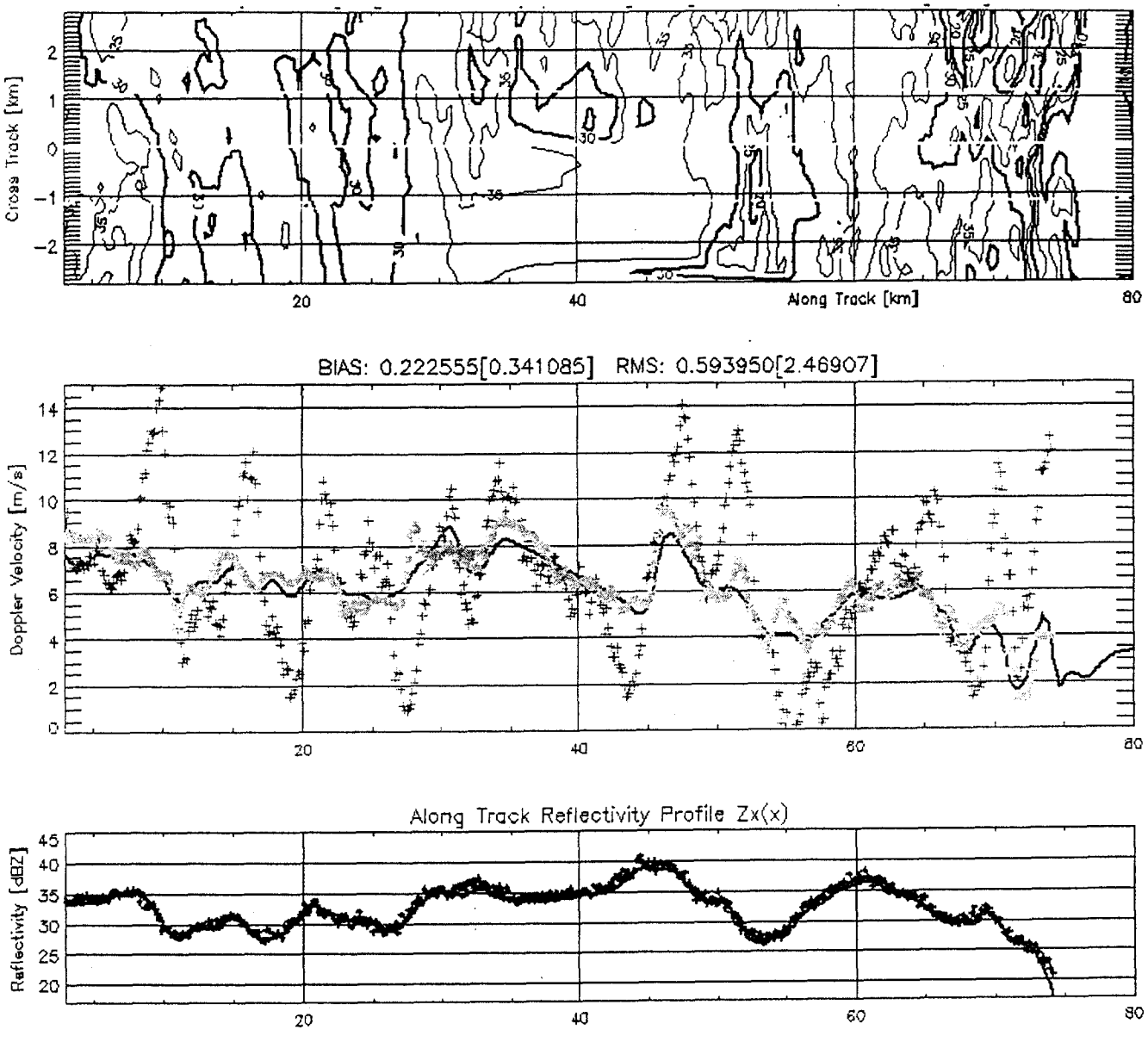

Fig. (4) Performance of DFT and CFT in a real case. Top: horizontal section of the reflectivity pattern (contour lines indicate dBZ). Center: as in Fig. (3) but light grey x indicate CFT estimates, and the statistical parameters are written without brackets; bracketed values and grey + describe DFT estimates. Bottom: as in Fig(3).

5. CONCLUSIONS AND COMMENTS

Three different techniques were applied in order to retrieve vertical velocity estimates of rainfall from a spaceborne Doppler radar. The standard PP and DFT are capable of providing accurate estimates when the rainfall field within the radar IFOV is almost uniform. The comparison of their performances shows a slightly better behavior of the latter under the considered configuration, although it must be highlighted that reduction of M or increase of PRF would improve the PP performances relatively to DFT. Both techniques are heavily affected by eventual non-uniformity of the rainfall pattern in the along-track direction: in this case the bias introduced by the unknown position of the 'center of mass' of the rainfall pattern respect to the satellite, cannot be reduced in any way by simply increasing M, PRF or Q.

A third technique (CFT) has been devised in order to mitigate the NUBF effects on vertical velocity estimates. It requires a sampling strategy that oversamples in the along-track direction (i.e., samples are taken for overlapping IFOVs). In this way it is possible to estimate the actual position of the strong reflectivity cells smaller than the IFOV, and therefore correct the bias introduced in the velocity estimates.

Simulations performed using a 3D Doppler simulator on actual measurements obtained by the airborne ARMAR radar show that NUBF effects can be almost cancelled by means of CFT, and therefore reliable estimates of vertical velocity can be obtained also for convective systems with rainfall cells smaller than the radar IFOV.

6. Knowledgements

The research described in this paper was performed by the Jet Propulsion Laboratory, California Institute of Technology, under contract with the National Aeronautics and Space Administration.

7. References

1. Atlas D., Srivastava R.C. and Sekhon R.S., Doppler Radar characteristics of precipitation at vertical incidence. Rev. Geophys. Space Phys. 2, pp.1-35, 1973
2. Doviak R.J. and Zrnic D.S., Doppler radar and weather observations, Academic Press, 1984, ISBN 0-12-221422-6
3. Amayenc P, et al. Proposal for a spaceborne dual-beam rain Radar with Doppler capability, J. Atm. Oce. Tech., 10, June 93, pp.262-276
4. Meneghini R and Kozu T., Spaceborne Weather Radar, Artech House Ed., 1990, ISBN 0-89006-382-6
5. Durden S.L., et al, Effects of NonUniform Beam Filling on rainfall retrieval for the TRMM Precipitation Radar, J. Atm. Oce. Tech., 15, Jun. 1998, pp. 635-646
6. Zrnic D.S., Estimation of spectral moments for weather echoes, IEEE Trans. On Geosc. Electr., 4, Oct. 1979, pp.113-128
7. Goodman J.W., Some fundamental properties of speckle, J. Opt. Soc. Am, Vol. 66, N 11, pp. 1145-1150, Nov 1976
8. Marshall J.S. and Hitschfeld W., Interpretation of the fluctuating Echo for randomly distributed scatterers. Part I, Can. J. Phys., 31, pp.962-995, 1953
9. Mahapatra P.R and Zrnic D.S., Practical Algorithms for Mean Velocity Estimation in Pulse Doppler Weather Radars Using a small number of samples, IEEE Tr. Geo. Rem. Sens., GE-21, N. 4, p.491-501, October 1983
10. Dias J.M.B and Leitao J.M.N, Nonparametric estimation of mean Doppler and spectral width, IEEE Trans. Geo. Rem. Sens., 38, pp.271-282, Jan. 2000
11. Sirmans D. and Bumgarner B., Numerical comparison of five mean frequency estimators, J. App. Met., 14, pp.991-1003, Sep.1975
12. Berger T. and Groginsky H.L., Estimation of the spectral moments of pulse trains, presented at the Int. Conf. On Inform. Theory, Tel Aviv, Israel, 1973